Spectrum extraction from detector plane images for the medium-resolution spectrometer of the mid-Infrared Instrument on-board the James Webb Space Telescope

Ioannis Argyriou, Ruymán Azzollini, Bart Vandenbussche

Ioannis Argyriou, Ruymán Azzollini, Bart Vandenbussche, "Spectrum extraction from detector plane images for the medium-resolution spectrometer of the mid-Infrared Instrument on-board the James Webb Space Telescope," Proc. SPIE 10698, Space Telescopes and Instrumentation 2018: Optical, Infrared, and Millimeter Wave, 106983L (6 July 2018); doi: 10.1117/12.2312697

SPIE.

Event: SPIE Astronomical Telescopes + Instrumentation, 2018, Austin, Texas, United States

Spectrum extraction from detector plane images for the medium-resolution spectrometer of the Mid-Infrared Instrument on-board the James Webb Space Telescope

Ioannis Argyriou[a], Ruymán Azzollini[b], and Bart Vandenbussche[a]

[a]Institute of Astronomy KU Leuven, Celestijnenlaan 200D,3001 Leuven, Belgium
[b]Department of Space and Climate Physics University College London, Gower Street, Bloomsbury, London WC1E 6BT, United Kingdom

ABSTRACT

The Mid-Infrared Instrument (MIRI) on-board the James Webb Space Telescope (JWST) performs medium-resolution spectroscopy in the 5 to 28.5micron wavelength range. In this paper two algorithms are presented that will be used to extract 1D spectra from the 2D absolutely calibrated detector science frames acquired with the Medium-Resolution Spectrometer (MRS) of MIRI. The first spectral extraction algorithm performs standard aperture photometry on point and extended sources. The second algorithm, applicable only to point sources, uses the instrument point spread function (PSF) and the pixel signal variance as a weighting function, to extract the signal from the detector pixels in an optimized way. This "optimal" extraction is also optimal in the case of faint source observations. The two algorithms are tested on MIRI ground test data and compared. For point sources, the optimal extraction algorithm is found to be more reliable than the aperture extraction algorithm.

Keywords: JWST, MIRI, mid-infrared, medium-resolution spectroscopy, spectral extraction, aperture photometry

1. INTRODUCTION

Light entering the medium-resolution spectrometer (MRS) of the mid-infrared instrument (MIRI) on-board the James Webb Space Telescope (JWST) is spectrally separated into four channels by dichroic mirrors [1, 2]. Each channel has its own integral-field-unit (IFU), and each IFU incorporates an image slicer. This structural component slices the field of view (FOV) of the MRS into a defined number of slices. The slices are used as entrance slits for the spectrometer, and each slit is imaged, thanks to a diffraction grating assembly (DGA), as a dispersed stripe on one of the halves of the MIRI detector arrays.

Four MRS channels are observed simultaneously in one exposure, however each exposure yields but a third of the total wavelength range of MIRI. To both cover the large wavelength range of MIRI (5 to 28.5microns) and achieve a spectral resolution of a few thousands, three exposures are required in three different grating settings. Each of the grating settings is called a subchannel (A, B, C), and with the four MRS channels covered (1, 2, 3, 4), there are 12 MRS spectral bands in total. From lower to higher wavelengths these bands are: 1A, 1B, 1C, 2A, 2B, 2C, 3A, 3B, 3C, 4A, 4B, 4C. The MRS wavelength coverage per spectral band is shown in Fig. 1 [3].

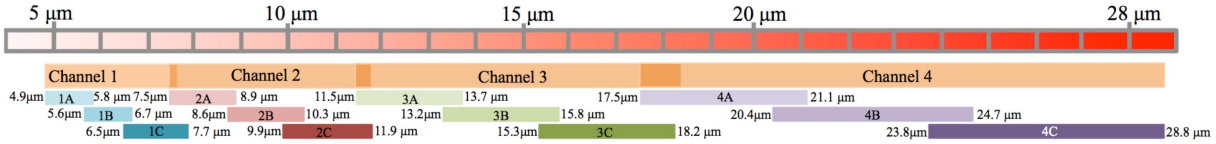

Figure 1. MRS wavelength coverage per spectral band.

Further author information: (Send correspondence to Ioannis Argyriou)
Ioannis Argyriou: E-mail: ioannis.argyriou@kuleuven.be, Telephone: +3216373310

Space Telescopes and Instrumentation 2018: Optical, Infrared, and Millimeter Wave, edited by Makenzie Lystrup, Howard A. MacEwen, Giovanni G. Fazio, Proc. of SPIE Vol. 10698, 106983L
 · doi: 10.1117/12.2312697

2. MRS DETECTOR IMAGES

In Fig. 2 two typical MRS detector images are shown. The detector images were obtained during a MIRI flight-model (FM) test campaign at the Rutherford Appleton Laboratory (RAL, England). The detector images shown are calibrated for the various effects applicable to MRS data (see [3]). The pixel signal is given in units of milliJansky per pixel. The detector image on the left is acquired from an 800 Kelvin (K) blackbody (BB) extended source observation. The detector image on the right is acquired from an 800K BB point source observation. The illumination pattern of the extended source is uniform, as shown by the homogeneous illumination of the different stripes on the detector. The IFU slicer "along-slice" direction is given here as the horizontal part of each respective stripe on the detector, while the dispersion direction is plotted along the vertical axis. The shape of the point source is spatially separated by the IFU image slicer. The separation between the different illuminated portions on the detector is due to the fact that nearby stripes on the detector are not nearby slices on the IFU slicers. In fact IFU slices are interleaved on the detector, as illustrated in Fig. 3.

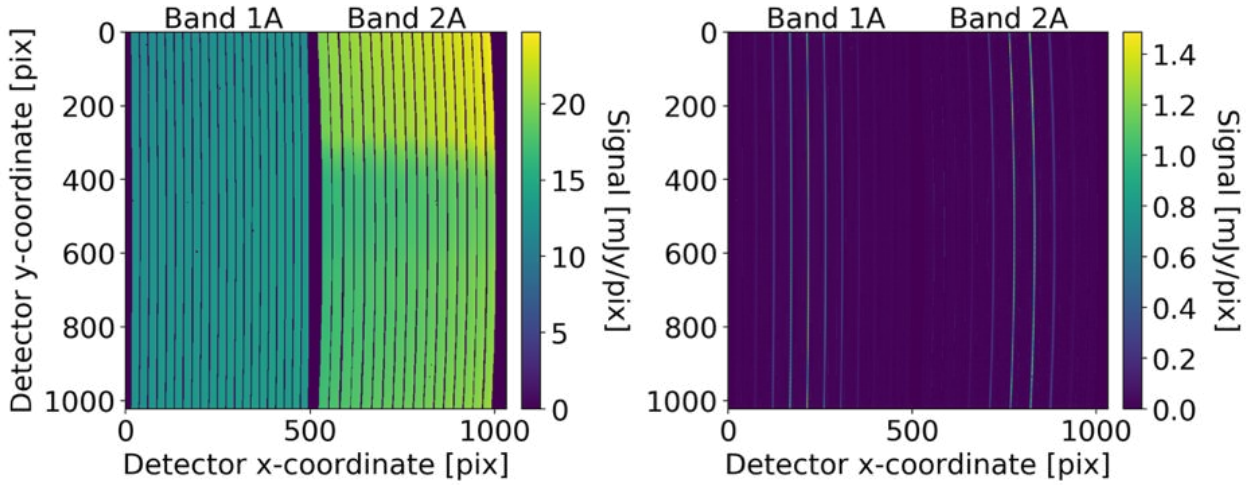

Figure 2. MRS observation of an 800K blackbody extended source (left) and of an 800K blackbody point source (right) in two MRS spectral bands. ach MRS IFU slices the MRS FOV into a number of slices. The slices are used as entrance slits for the spectrometer, and each slit is imaged, thanks to a diffraction grating, as a dispersed stripe on one of the halves of the MIRI detector arrays.

As mentioned, a movement on the horizontal axis within a given slice on the detector, is equivalent to a spatial movement, along a slice, on the IFU image slicer. A point on the IFU image slicer can, with the correct transformations, be expressed in terms of global telescope coordinates. The definition of a transformation matrix between the detector, the image slicer reference frame, and the global telescope reference frame is not straightforward, and is a principal output of the calibration efforts of the MIRI consortium. This, together with the wavelength calibration of the MRS, constitutes the so-called "detector2cube" (D2C) calibration data product (CDP). This product is used to relate a given detector pixel's (x,y) position to a three-dimensional coordinate. Using α as the along-slice position on the IFU image slicer, β as the across-slice position on the slicer, and λ as the grating-projected wavelength on the detector, each detector pixel coordinate doublet (x,y) is related to an (α, β, λ) coordinate triplet. A visual representation of the slicer spatial coordinates (α, β) is given in Fig. 4.

For a given MRS spectral band, provided a D2C transform, an (α, β, λ) map can be adopted for the part of the detector where the spectral band is projected. This is shown for MRS spectral band 1A in Fig. 5. The along-slice position and the across-slice position are given in units of arcseconds. Wavelengths are given in units of microns. The values of α and λ vary continuously within a slice, while the values of β are discrete. The reason why β is given a unique value in each slice is related to the working principles of the MRS IFU, and how the MRS optics sample the MRS FOV.

An IFU allows for the reconstruction of three-dimensional (3D) spectral cubes from 2D plane detector images. The three-dimensions correspond to two spatial directions on the sky and one dispersion direction. For the

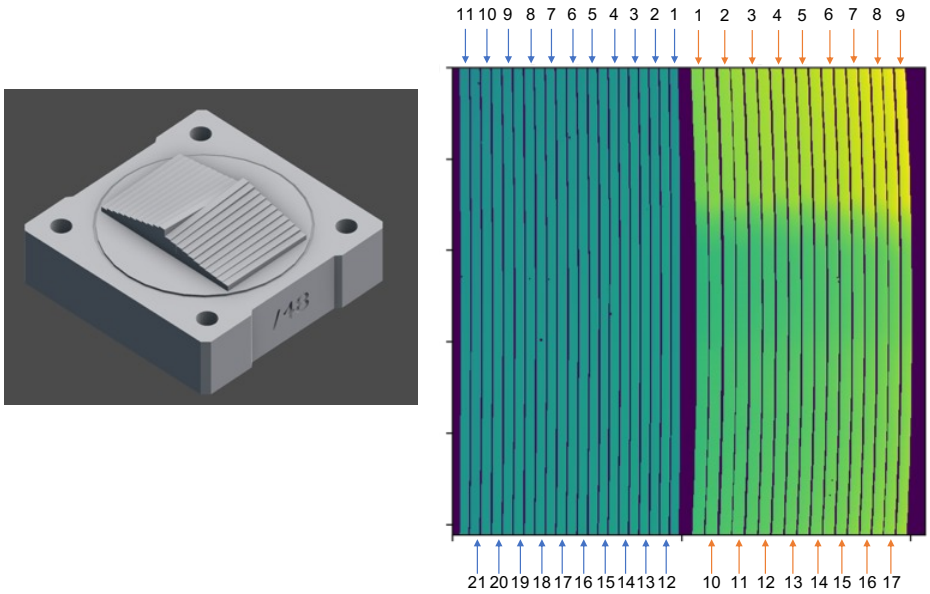

Figure 3. (Left) Artistic representation of MRS IFU image slicer. The engraved IFU slices are tilted with respect to one another. (Right) Order of MRS IFU slices as projected on the MIRI detector by the MRS diffraction gratings. The MRS channel 1 IFU image slicer is divided into 21 slices. The MRS channel 2 IFU image slicer is divided into 17 slices. Slice number 1 represents one edge of the image slicer, while slice number 21 (or 17) represents the opposite side of the slicer.

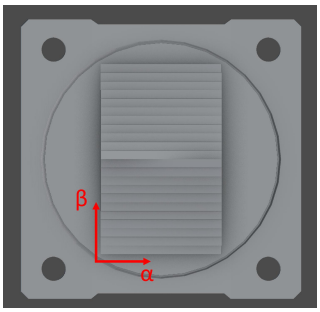

Figure 4. MRS IFU slicer coordinates on a fictitious image slicer. The symbol α is used for the along-slice position. The symbol β is used for the across-slice position.

purposes of this work the MRS local spatial coordinates (α, β) are used as the two spatial directions. Spatial pixels in the cube are abbreviated as "spaxels". The number of spaxels in the across-slice direction β is defined by the design of the IFU slicer. For instance the MRS channel 1 IFU slicer has 21 slices, thus the reconstructed spectral cubes of MRS channel 1 have 21 spaxels in one spatial direction. The number of spaxels in the perpendicular direction, the along-slice direction α, is determined by the spatial resolution achieved by the JWST telescope and MRS optics. In Fig. 6 a single cube image layer is shown at a wavelength $\lambda = 5\mu m$. Note that a MRS 3D spectral cube contains a large number of layers, proportional to the achieved MRS spectral resolving power.

In section 3 the methodology and rationale in extracting spectral information from 2D plane detector images instead of reconstructed 3D spectral cubes is described. In section 4 the methodology presented in section 3 is applied to MRS images taken during ground tests.

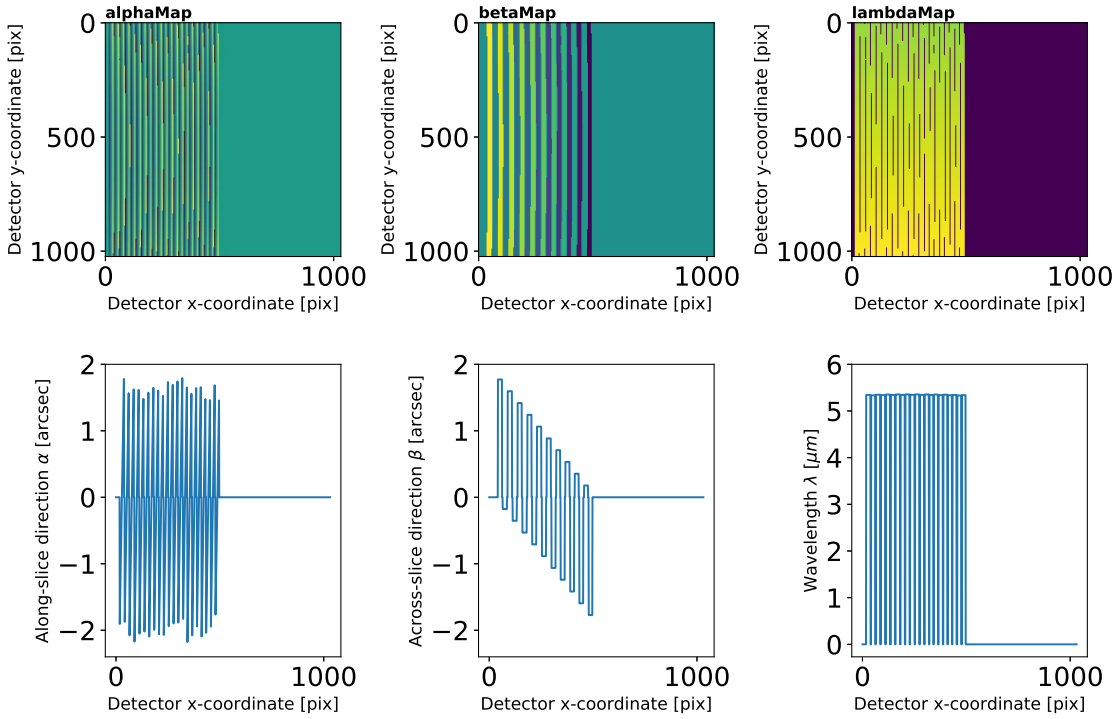

Figure 5. (Top) MRS detector pixel-corresponding (α, β, λ) map in MRS spectral band 1A. (Bottom) Horizontal cross-section of atop 2D images, at the middle of the detector (pixel row 512).

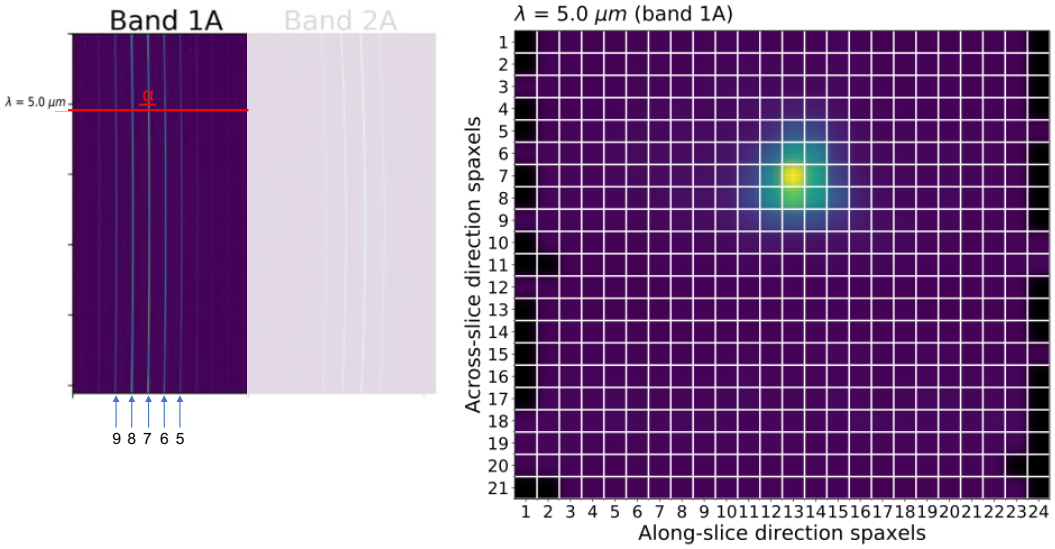

Figure 6. Reconstruction of MRS 3D spectral cube from 2D plane detector image of a point source. Spatial pixels in the cube are abbreviated as "spaxels". The number of spaxels in the vertical direction (across-slice direction) is defined by the design of the IFU slicer. A single cube image layer is shown at $\lambda = 5\mu m$. The slice identifiers (5, 6, 7, 8, 9) on the detector image (left) match the same spaxel row identifiers on the cube image (right).

3. MRS DETECTOR SPECTRAL EXTRACTION

The calibration pipeline of the MIRI MRS provides to the end-user 2D detector images and 3D spectral cubes of observed sources. The pipeline allows to extract a 1D spectrum from either of the two data products. The process for reconstructing 3D spectral cubes involves interpolating the 2D detector data onto a regular grid, thus a case is made for extracting 1D spectra from 2D detector images rather than extracting 1D spectra from reconstructed 3D spectral cubes based on two reasons:

1. By extracting 1D spectra directly from 2D detector images, unwanted variance correlations between spaxels are avoided.
2. In case of low signal-to-noise observations, interpolating noisy data before the extraction can also be avoided.

Two different algorithms are developed to perform the 1D spectral extraction from 2D plane detector images. The first algorithm is termed "aperture extraction" and is based on the technique of aperture photometry, while the second algorithm is termed "optimal spectral extraction". Aperture extraction, described in subsection 3.1, is a method applicable to both point source and extended source MRS observations. Conversely, optimal spectral extraction described in subsection 3.2 is applicable only to point source observations. First the aperture extraction algorithm is described.

3.1 Aperture extraction from 2D detector images

The basic principle of aperture extraction is to define a shape of prescribed dimensions (e.g. circle, ellipse, rectangle), and identify all the pixels/spaxels that fall within said shape. This is easily illustrated in the 3D spectral cube case, as shown in Fig. 7. All spaxels within the outline circle or rectangle are used to extract the signal from the source. Although the imagining is a bit more complex for the case of the 2D MRS detector images, the working principle is the same, in that the detector pixels that fall within a spatially-defined aperture have to be identified.

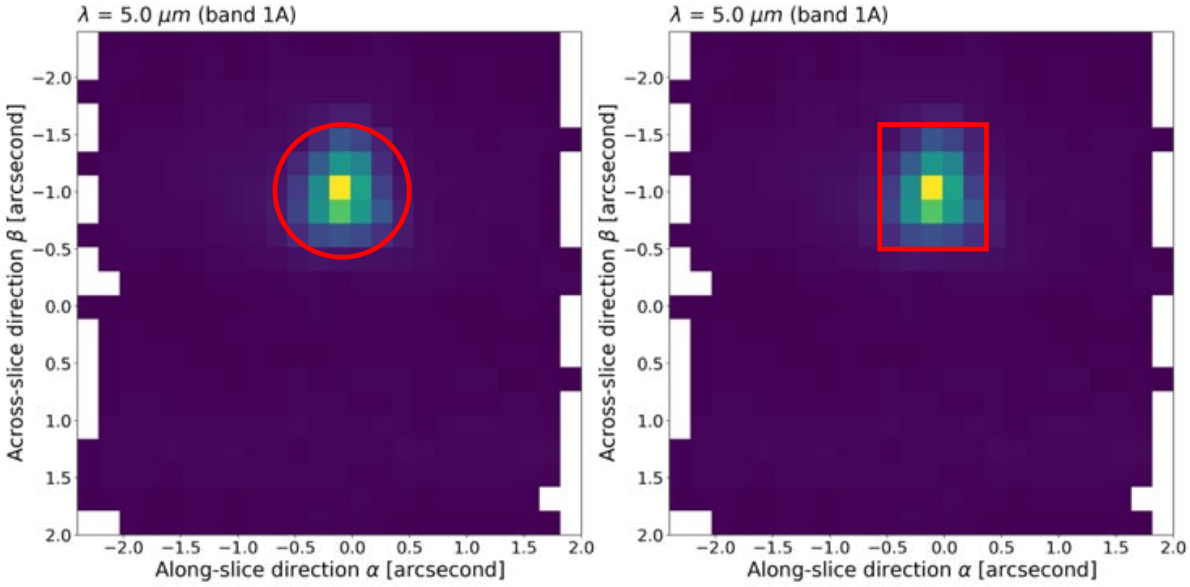

Figure 7. Example of how aperture extraction is applied on a layer of a 3D MRS reconstructed spectral cubes for the case of a circular aperture (left) and a square aperture (right).

To define an aperture in pixel space, the (α,β) maps shown in Fig. 5 are used. Fig. 8 shows an example of which pixels satisfy a circular aperture criterion, as given by Equ.1.

$$(\alpha_{pix} - \alpha_{cen})^2 + (\beta_{pix} - \beta_{cen})^2 \leq R^2 \tag{1}$$

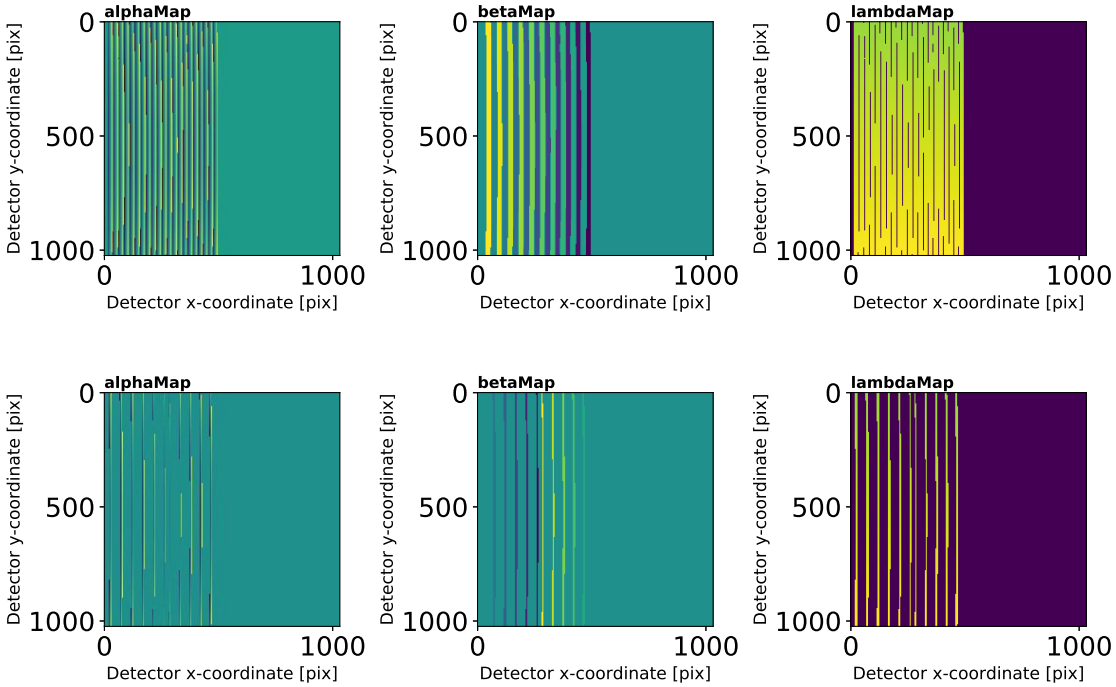

Figure 8. Top: Original (α, β, λ) pixel coordinate maps in MRS spectral band 1A. Bottom: (α, β, λ) coordinate maps with pixels falling within a circular aperture with a radius of 1 arcsecond, centered at $(\alpha_{cen}, \beta_{cen}) = (0, 0)$ arcseconds.

As illustrated in Fig. 8, the aperture definition works both spatially and spectrally on the MRS detector image data. That is because no explicit spectral information is contained in the aperture definition. To parallel the intuitive image of applying the aperture extraction on a cube layer as shown in Fig. 7, it should be mentioned that a cube layer is formed by using detector pixels that belong to a "spectral bin" on the detector. Put simply, a spectral bin has a central wavelength λ_c and a spectral width $\Delta\lambda$. In the case of the MRS detector images, a spectral bin encompasses all dispersed stripes on the detector. A spectral grid, formed from a collection of bins, is derived based on an iterative scheme. This scheme loops over Equ.2 and Equ.3.

$$\Delta\lambda = \frac{\lambda_0}{Resolving\ power} \tag{2}$$

$$\lambda_{cen} = \lambda_0 + \frac{\Delta\lambda}{2} \tag{3}$$

where initially λ_0 is the smallest wavelength considered for a specified MRS spectral band $\lambda_{band,min}$. Equ.2 and Equ.3 are then looped over until $\lambda_{cen} > \lambda_{band,max} - (\Delta\lambda/2)$, at which point the iterative scheme is terminated. Given a spectral bin's central wavelength λ_{cen} and spectral width $\Delta\lambda$, the pixels belonging to a spectral bin can be determined via the detector wavelength map shown in the top right plot of Fig. 8. An example of a spectral bin in the MRS spectral band 1A is shown in Fig. 9. It is by interpolating the signal of these pixels that a cube layer, such as the one shown in Fig. 7, can be formed.

The aperture extraction algorithm works on the detector by masking pixels based on their spatial information, and the aperture extraction is applied iteratively in each spectral bin. Depending on whether the observed source is an extended or a point source, the pixel signals are summated accordingly.

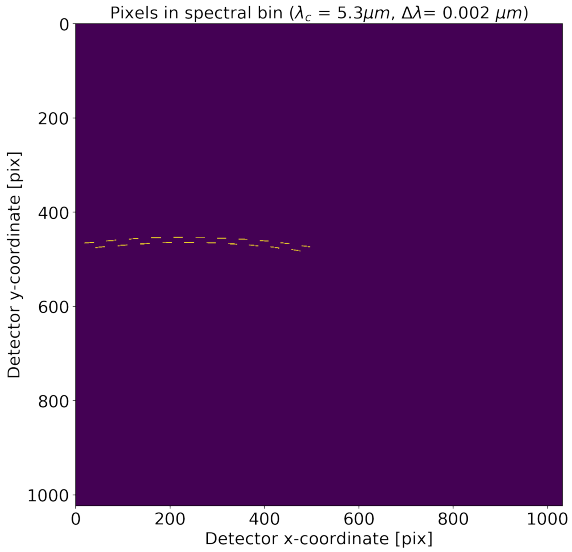

Figure 9. Spectral bin on the detector (MRS spectral band 1A).

In the case of an extended source observation, the aperture extraction algorithm works as follows:

1. For each pixel on the detector, within the illuminated stripes, the solid angle subtended on the IFU slicer is computed in units of $arcsec^2$. This is done using the spatial coordinates (α, β) at the pixel corners, and Heron's formula for the area of a quadrilateral. The area of a quadrilateral is used instead of a rectangular shape to compensate for the distorted shape of the MRS slices, caused by the slicing optics.
2. The signal of each pixel identified in step 1 is divided by the solid angle covered by said pixel. This means that the signal units are converted from milliJansky per pixel, to milliJansky per $arcsec^2$, equivalent to units of surface brightness.
3. An aperture of user-defined shape and size is defined.
4. The aperture is used to mask unwanted pixels. This step is performed in every spectral bin.
5. The signal of the unmasked pixels defined in step 4 is summed in every spectral bin.
6. The summed signal in a spectral bin is divided by the number of unmasked pixels in the spectral bin.
7. The averaged signal computed in step 6 is multiplied by the area of the user-defined aperture. The final signal values are given in units of milliJansky, i.e. in units of spectral flux density or spectral irradiance.

Considering a point source observation, an important aspect of the observation is in how the centroid of the source is estimated. This centroid informs the aperture center coordinates $(\alpha_{cen}, \beta_{cen})$, and thus having a robust centroiding algorithm is essential, to minimize the amount of background signal taken in as science signal. To that end a point source centroiding algorithm has been developed, to determine the point source center from 2D MRS detector images. The centroiding algorithm works in three steps:

1. A rough centroid is estimated by finding the stripe on the detector with the highest integrated signal. Recall that each stripe on the detector is equivalent to a discrete across-slice position β_{cen}. Subsequently, within the stripe with the highest integrated signal, the along-slice position α of the pixels with the highest signal are used to approximate the along-slice centroid of the point source. This yields a zeroth estimate for the point source centroid $(\alpha_{cen}, \beta_{cen})$.

2. In the stripe with the highest integrated signal determined in step 1, in every spectral bin, a Gaussian distribution is fitted to the along-slice profile of the signal. This yields an optimized value of the wavelength-dependent source along-slice position $\alpha_{cen,bin}$. By finding the pixel in each detector stripe and spectral bin with an along-slice position closest to $\alpha_{cen,bin}$, a Gaussian distribution is fitted to the resulting signal profile, formed from the collection of the identified pixels. This yields an optimized source across-slice position$\beta_{cen,bin}$. An example of the result of this step is shown in Fig. 10.

3. Each pixel in a spectral bin has a corresponding $(\alpha_{pix}, \beta_{pix})$ coordinate, and these coordinates can be used to make a non-regular spatial grid. Using the optimized $(\alpha_{cen,bin}, \beta_{cen,bin})$ coordinates determined in step 2, a global 2D Gaussian fit is made to all the pixels in the non-regular spatial grid. An example of the result of this step is shown in Fig. 11.

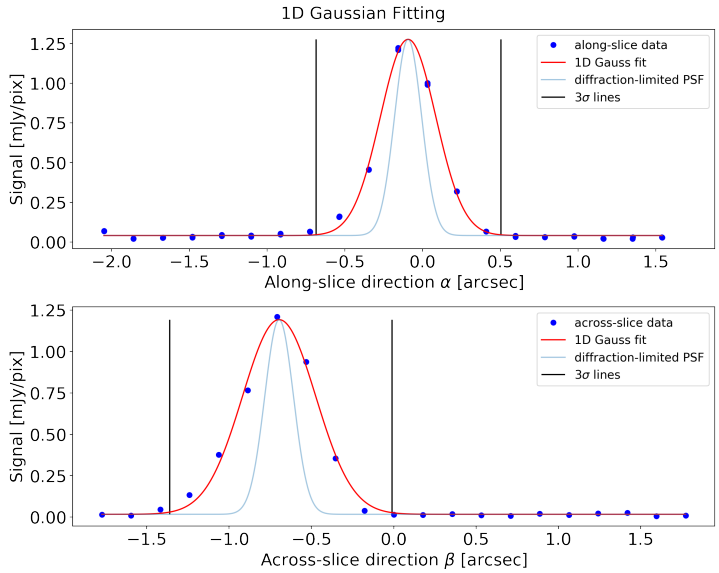

Figure 10. Optimized 1D point source centroiding in MRS band 1A, in spectral bin centered at $5.3\mu m$. The optimization is based on a 1D Gaussian distribution fit in the along-slice and across-slice directions, shown in the top plot and the bottom plot respectively. The theoretical diffraction-limited point-spread function (PSF) of the MRS is also shown, illustrating that the observed point source is not point-like, but is slightly extended.

The determined source centroid is used to center the user-defined aperture for aperture extraction. The aperture extraction algorithm then applies the following steps:

1. An aperture of user-defined shape and size is defined.

2. The aperture is used to mask unwanted pixels. This step is performed in every spectral bin.

3. The signal of the unmasked pixels defined in step 2 is summed in every spectral bin. The final signal values are given in units of milliJansky.

Two corrections have to be applied to the above point-source-derived signal. The first correction has to do with the differential spectral sampling of the MRS. Different spectral bins on the detector yield different amounts of pixels on the detector. This is shown for all the MRS spectral bands in Fig. 12. The observed effect is caused by the spectral oversampling imposed by the MRS optics across the different bands.

Since each pixel subtends a solid angle on the MIRI focal plane, the effect shown in Fig. 12 effectively results in a systematic scaling in the signal measured by the aperture extraction algorithm. In order to impose flux

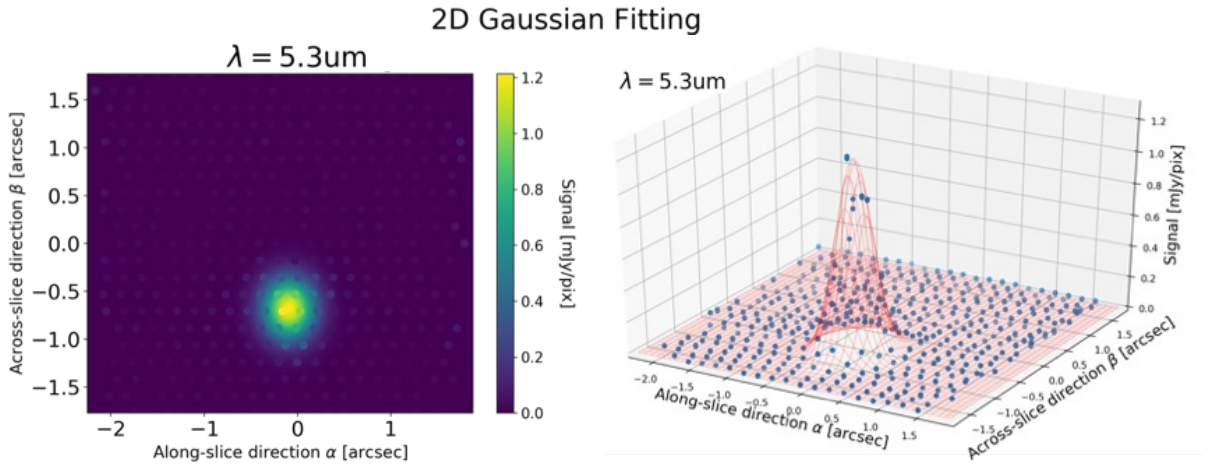

Figure 11. Optimized 2D point source centroiding in MRS band 1A based on 2D Gaussian distribution, fit in along-slice and across-slice directions simultaneously. The left plot is a scatter plot of the pixel spatial values and signal values in a spectral bin. The right plot is a wireframe version of the left plot.

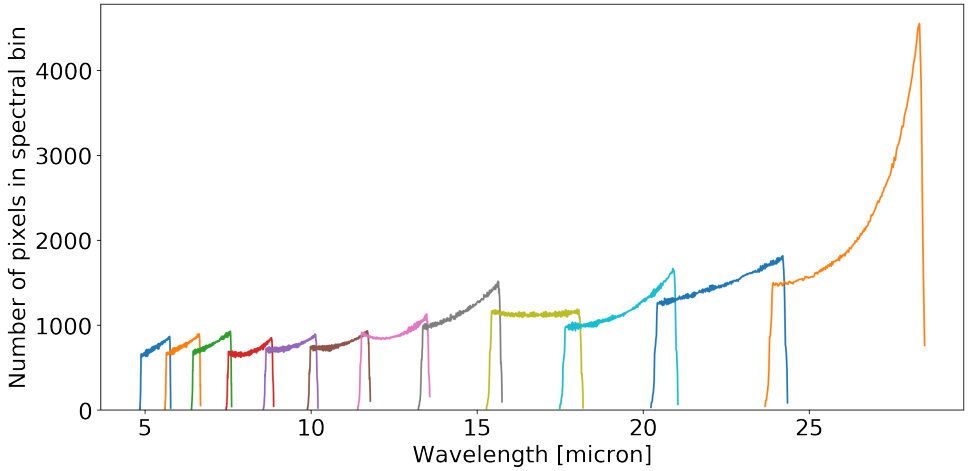

Figure 12. Number of pixels that contribute to a spectral bin on the MRS detector. Each MRS spectral band is represented with a different color. There are 12 spectral bands in total.

conservation on the derived signal, a normalization factor is computed for each spectral bin. The factor is defined as a ratio of the summated solid angle subtended by the pixels in a spectral bin, divided by a reference solid angle, which is calculated as $(\alpha_{max} - \alpha_{min}) \cdot (\beta_{max} - \beta_{min})$ in the same spectral bin. The resulting normalization factor is shown in Fig. 13. Given the Nyquist sampling criterion of two samples per resolution bin (shown as the horizontal dashed line), one notices that the MRS is spectrally undersampled below 10 micron, ideally sampled between 10 and 12.5micron, and spectrally oversampled above 12.5 micron.

The second correction applied to the signal extracted for point sources is the application of an "aperture correction" factor. Provided a choice for an aperture shape and size, it is difficult to optimize this choice based on a need to minimize the background signal, while at the same time accounting for as much of the source signal as possible. If the instrumental PSF is well-known however, an aperture correction factor can be applied to the extracted signal. Provided that the PSF is normalized to unity, as shown in Equ.4, the aperture correction factor (AC) is defined in every spectral bin according to Equ.5.

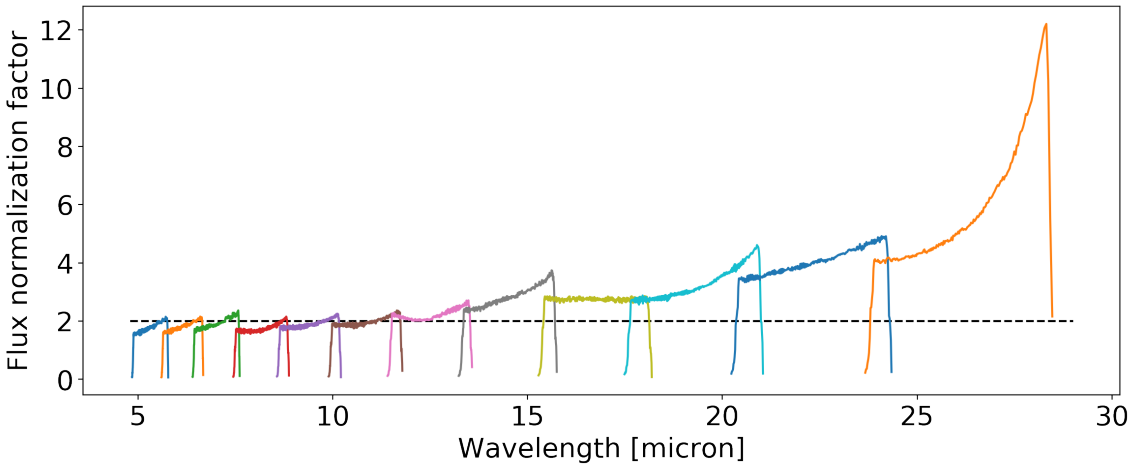

Figure 13. Flux normalization factor determined from the summated solid angle of the pixels in a spectral bin, divided by a reference solid angle calculated as $(\alpha_{max} - \alpha_{min}) \cdot (\beta_{max} - \beta_{min})$ in the same spectral bin. The dashed horizontal black line represents the Nyquist sampling criterion of two samples per resolution bin.

$$\int_{\alpha}\int_{\beta} P_{\lambda_{bin}} = 1 \tag{4}$$

$$AC_{\lambda_{bin}} = 1 - \frac{\int\int_{aper} P_{\lambda_{bin}}}{\int_{\alpha}\int_{\beta} P_{\lambda_{bin}}} \tag{5}$$

"P" denotes the PSF values in the spectral bins, denoted as "λ_{bin}". The aperture correction $AC_{\lambda_{bin}}$ has a value less that 1, and is used as a multiplicative factor on the extracted signal. The resulting fraction of the signal is then added to the extracted signal. How the PSF is used in the context of MRS point source spectral extraction is explained in the next section.

3.2 Optimal spectral extraction

The optimal spectral extraction algorithm is so-termed "optimal" because it uses the known point source distribution in the MRS slices and the pixel signal variance to maximize the extracted signal and minimize the added noise. The method described is based on the algorithm presented by Keith Horne in [4], and operates as follows. If the instrumental PSF is well-known, the flux signal in a spectral bin (f_{bin}^{opt}) can be computed as a weighted sum of the pixel values in the spectral bin. Optimal weights are computed in such way as to minimize the variance of the extracted pixel signal values. Quantitatively:

$$f_{bin}^{opt} = \frac{\sum_x W_{x,\lambda_{bin}} \cdot p_{x,\lambda_{bin}} / P_{x,\lambda_{bin}}}{\sum_x W_{x,\lambda_{bin}}} \tag{6}$$

where "opt" stands for "optimal", "x" is used in this case as a generic symbol for the spatial coordinates (α, β), and "p" denotes the pixel signal values. The optimization formula for the weights "W" is given by Equ.7.

$$\frac{1}{W_{x,\lambda_{bin}}} = var\left[\frac{p_{x,\lambda_{bin}}}{P_{x,\lambda_{bin}}}\right] = \frac{V_{x,\lambda_{bin}}}{P^2_{x,\lambda_{bin}}} \tag{7}$$

where "V" is the variance of the pixel measurements. Using these weights yields a variance on the flux measurement given by Equ.8.

$$var(f_{\lambda_{bin}}) = \frac{1}{\sum_x P^2_{x,\lambda_{bin}}/V_{x,\lambda_{bin}}} \tag{8}$$

Conceptually, the optimal extraction method imposes higher weights on pixel values with low-variance signal values (low uncertainty) closest to the PSF peak, and imposes lower weights on pixel values with high-variance (high uncertainty) furthest from the PSF peak. Considering some observational scenarios, for low signal-to-noise observations, the optimal extraction method allows to make the most out of the known PSF profile, to minimize the noise introduced into a spectrum. For high signal-to-noise observations with a clear PSF, variance on the pixel values is equal to the uncertainty in the PSF determination, thus the weights all equal to 1.

To apply the optimal spectral extraction algorithm on MRS IFU data, it is important to have:

- a representative PSF.
- representative estimates for the pixel signal variances.
- an accurate centroid for the source on which to center the PSF (based on centroiding algorithm presented in section 3.1).

These items are all products of the MRS calibration pipeline. Use is made of the MIRI MRS PSF CDP derived from ground test data, the pixel signal variance estimates provided by the pipeline, and the centroiding algorithm described in subsection 3.1.

The MRS PSF CDP provides the MRS instrumental PSF in a 3D spectral cube format. To extract detector pixel signals using the optimal spectral extraction method, the 3D PSF needs to be projected onto the 2D detector grid. Since the PSF is used as a weighting function for a point source distribution on the detector, the point source centroid is given as input to the PSF 2D projection step. The projection is performed by interpolating the 3D cube values to the (α,β,λ) detector pixel values. The result of the projection is shown for MRS band 1A in Fig. 14. Fig. 15 shows a horizontal cross-section (pixel row) of the spectrum shown in the right plot of Fig. 14 and the same row of the spectrum shown in the right plot of Fig. 2. By determining the centroid of the point source, the model PSF has been projected on the detector and overlaps the measured point source profile. The pixel signal variance, provided by the MRS calibration pipeline, is also overplotted in the figure. The projected PSF values and the pixel signal variance values are artificially scaled up for better visibility.

A 1D spectrum is extracted from the 2D detector image using Equ.6 and Equ.7. In the next section the optimal extraction algorithm and the aperture extraction algorithm are tested and compared.

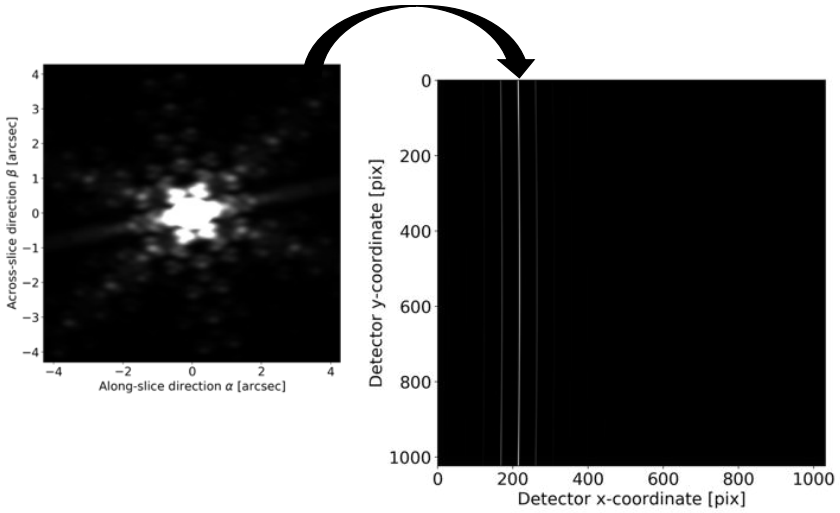

Figure 14. PSF projection in MRS band 1A from 3D spectral cube to 2D detector image. The projection is performed by interpolating the 3D cube values given in (α,β,λ) coordinates on the cube, to the (α,β,λ) coordinates of each detector pixel.

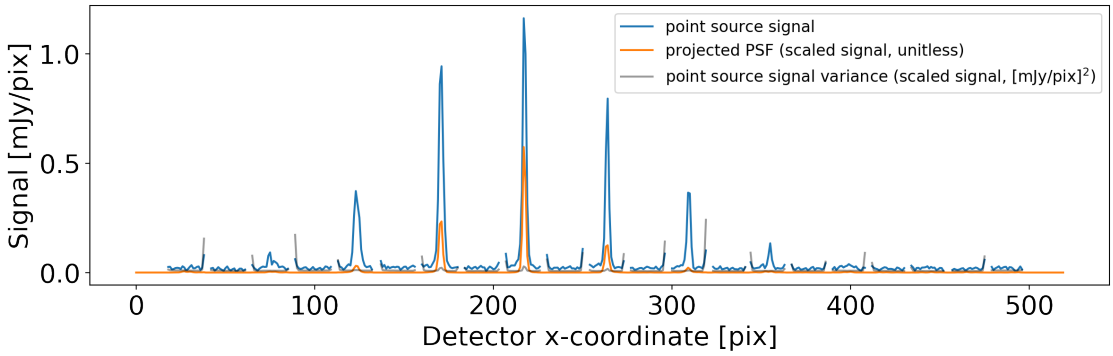

Figure 15. Comparison of MRS point source observation and projected PSF. The figure is taken from a horizontal cross-section of the spectrum shown in Fig. 2 and the spectrum shown in Fig. 14 (both right plots). By determining the centroid of the point source observation the model PSF is projected in such a way as to overlap the measured PSF. The pixel signal variance is also shown.

4. TESTING THE SPECTRAL EXTRACTION ALGORITHMS

The spectral extraction algorithms described in section 3 are used to extract 1D spectra from MRS detector plane images. This is done for three extended source configurations and one point source configuration. The data were acquired during the FM ground testing of MIRI at RAL. The optical stimulus, a blackbody source of configurable temperature, was provided by the MIRI Telescope Simulator (MTS). The MTS allowed to take both source measurements and background measurements with the MRS. The observational datasets include:

- A 400K, a 600K, and an 800K BB extended source observation in all 12 MRS spectral bands.
- An 800K BB point source observation in all 12 MRS spectral bands.
- Associated background measurements for each of the afore-mentioned observations.

The background measurements are subtracted from the source measurements before spectral extraction. The calibrated detector images for the three extended source temperature cases are shown in Fig. 16, in units of surface brightness.

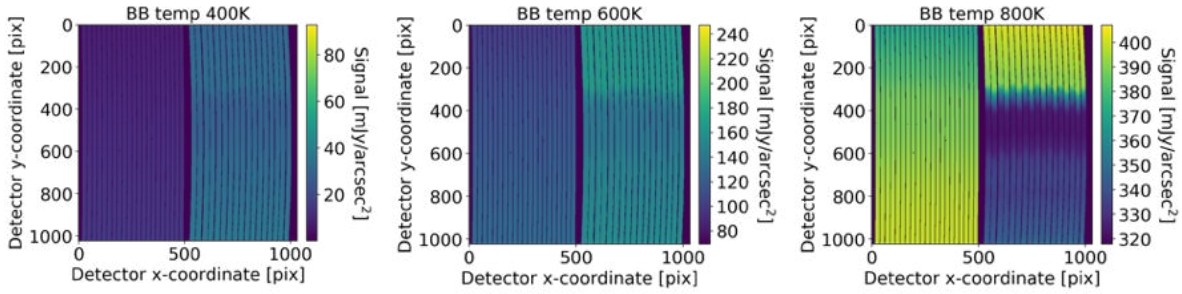

Figure 16. MRS detector images for three MRS observations of an extended blackbody source at three different temperatures. The images are shown in MRS band 1A/2A (left/right half of detector), and the pixel values are in units of surface brightness ($mJy/arcsec^2$).

The methodology described in subsection 3.1 is applied for the spectral extraction of an extended source scientific signal. This is done for all MRS spectral bands (band 1A to band 4C). A circular aperture with a radius of $1arcsec$ is used. The result of the aperture extraction is shown in Fig. 17. A water absorption feature is visible at $8.4\mu m$, caused by ice that formed during the cooling of MIRI, prior to the start of the tests. Slight discontinuities in the spectral continuum at the band edges are caused by small discrepancies in the calibration of the different MRS spectral bands. Noise in band 4C causes erratic spectral behavior, seen most clearly in the spectral profile of the 400K blackbody.

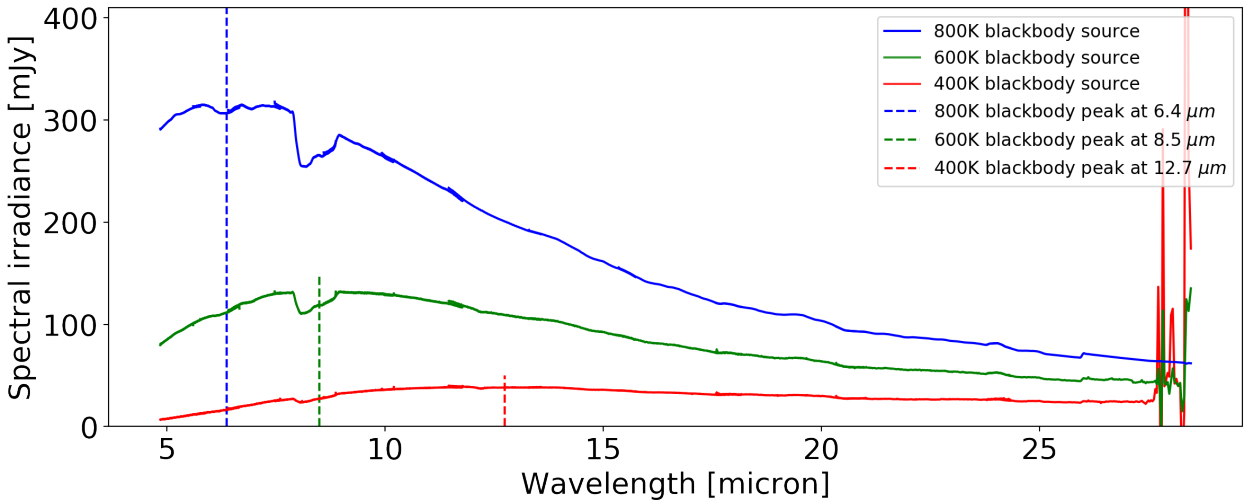

Figure 17. 1D extracted spectrum from spectral irradiance measurements at MIRI focal plane. The spectra were extracted using the aperture extraction algorithm on a series of detector images covering all spectral bands of the MRS.

To extract a 1D spectrum from the 800K BB point source observation, first the aperture extraction algorithm is used. In this case a circular aperture is used. The radius of the used aperture is specified as the radius required to achieve 80% encircled energy fraction of the instrumental PSF. By applying a series of circular aperture radii centered on the (normalized) PSF peak and summing the PSF signal in the aperture, a curve of growth is produced, as illustrated in Fig. 18. One can plot the 80% encircled energy fraction radius determined in every spectral bin to get a function of optimal aperture size versus wavelength. This is shown in Fig. 19. The overall

linear trend probes the diffraction broadening of the MRS instrumental PSF over the wavelength range covered by the MRS.

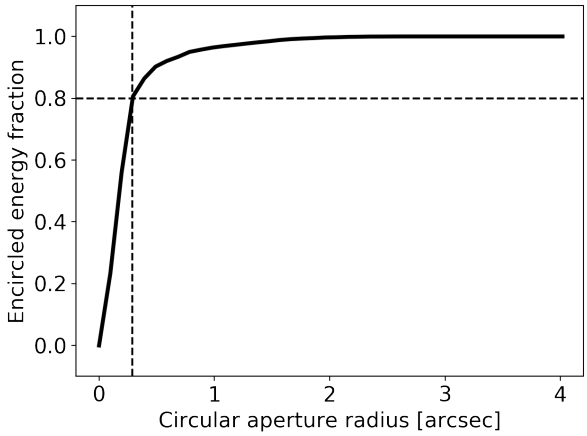

Figure 18. Encircled energy fraction for different aperture radii determined using the MRS instrumental PSF in MRS band 1A. In this example the 80% encircled energy fraction is achieved at a radius of 0.29 arcsec.

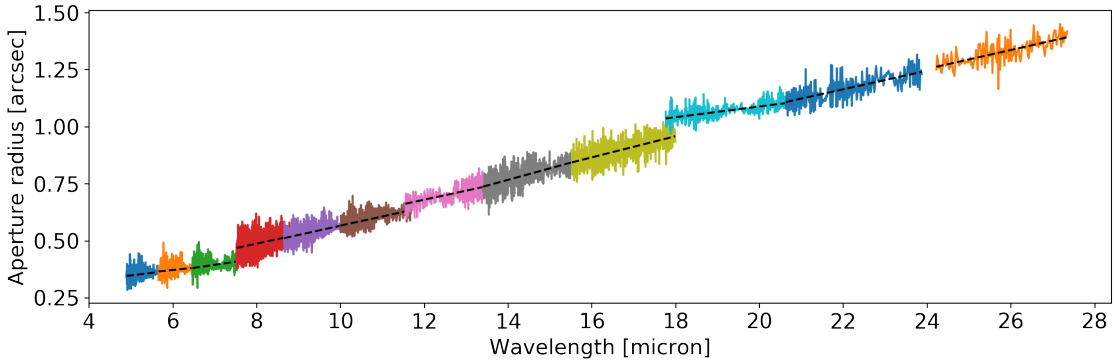

Figure 19. Circular aperture radius needed to achieve 80% encircled energy fraction of detector-projected MRS PSF. A dashed black line is overplotted in every spectral band, showing the linear regression of the data.

The aperture extraction algorithm is applied in every spectral bin of every MRS spectral band. A circular aperture is used to mask unwanted pixels that fall outside of the radius specified by the radius shown in Fig. 19. The pixel masking takes place on an all-or-nothing basis, meaning that if the spatial position of the center of a pixel falls inside the aperture then it is adopted into the signal, otherwise it is discarded. To position the aperture mask on the source centroid, the source centroid is determined in each spectral bin. Fig. 20 shows the determined along-slice position of the source, and Fig. 21 shows the determined across-slice position.

It is important to realize that the definition of the (α, β) coordinates is spectral-band-specific. "Where" light will fall on the detector depends on the optics placed before the detector. Since the optical train of each MRS spectral band is slightly different, the (α, β) coordinates of the point source are also different in each band. Note however that the mean position of a source in a spectral band should not change. Fig. 20 shows that there is a systematic error in the definition of the detector (α) reference map, itself acquired from the MRS D2C CDP. Pixels that should have the same (α) value regardless of wavelength, have (α) values that change as a function of wavelength. The origin of this calibration error is now understood and will be corrected in an upcoming version of the D2C CDP. Fig. 21 shows that the across-slice position of the source is much better constrained, albeit the uncertainty is large at the longest spectral bands (4B and 4C).

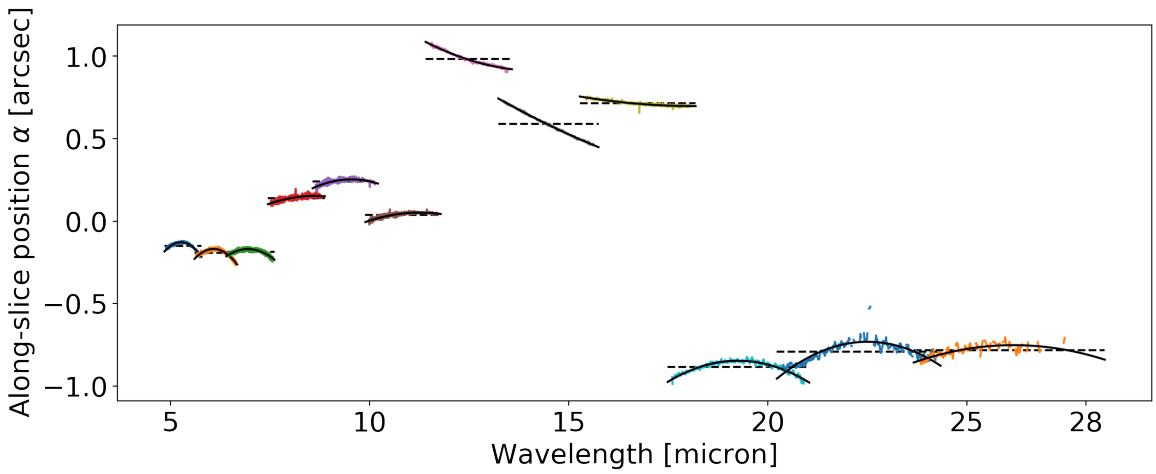

Figure 20. Along-slice position of 800K BB point source. The solid black line represents a second-order polynomial fit to the source along-slice position, while the dashed black line shows the mean position of the source in a spectral band.

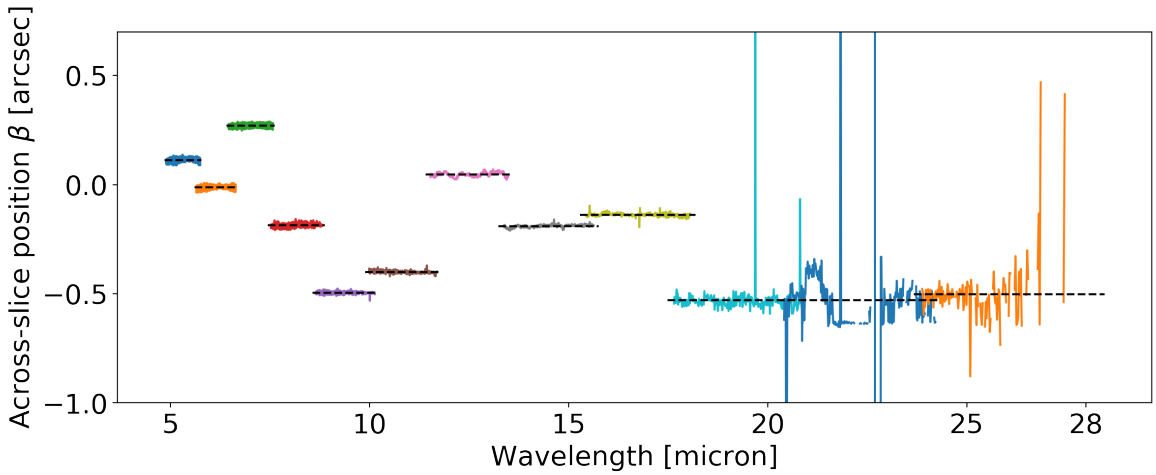

Figure 21. Across-slice position of 800K BB point source. The dashed black line shows the mean position of the source in a spectral band.

The center of the circular aperture is matched to the point source centroid, and the aperture radius has been defined based on the 80% PSF encircled energy fraction. The aperture extraction algorithm is used on the point source detector images using the aperture inputs. The result is shown in Fig. 22. The extracted signal shows clear edge effects in the first few and last couple of spectral bins in each spectral band. One notices the drop in signal between 21 microns and 23 microns. This is caused by localized negative signal in the detector image signal. Uncorrected systematic errors in the MRS calibration of each pixel value manifest across the spectrum. One such error is introduced by fringing in the detector images (see [2]), appearing as high-frequency noise modulating the spectral continuum. The current fringe calibration works well for extended sources, as illustrated by the absence of fringes in Fig. 17. An accurate fringe correction for point source observations however is still work in progress. Background signal from the test environment can also contribute noise to the spectrum, and this can be seen in Fig. 22 by the increasingly erratic signal beyond 26 microns.

Optimal spectral extraction, presented in subsection 3.2, is used on the same point source observations. The result is shown in Fig. 23. Qualitatively the signal extracted appears similar to the aperture extracted spectrum. In order to compare the result of the aperture and the optimal extraction algorithm, the spectra derived from

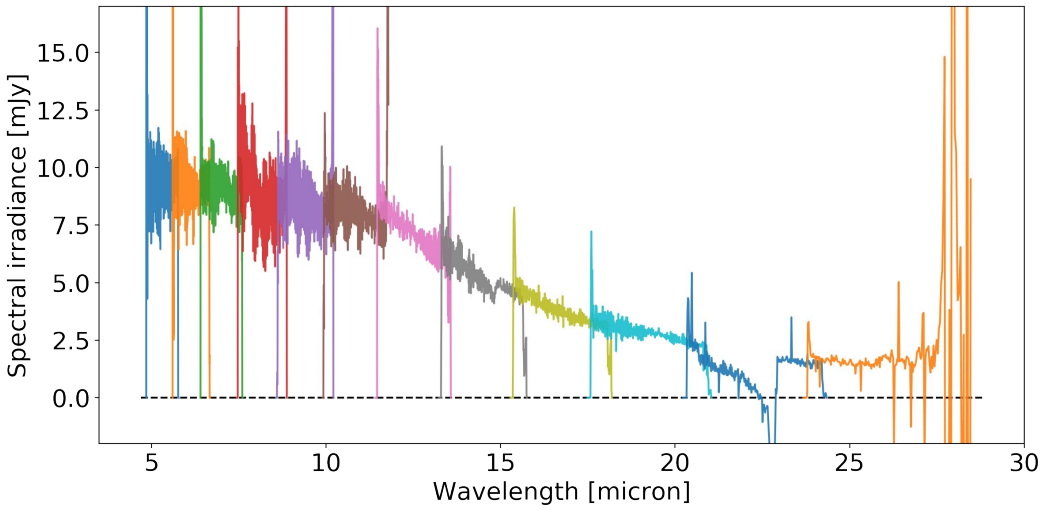

Figure 22. 800K BB point source aperture extracted signal.

both approaches are overplotted in Fig. 24. It was mentioned in subsection 3.2 that if a point source observation yields a clear PSF, such as is the case here, then the two algorithms will yield similar results. This is what is shown in Fig. 24. Nevertheless the longest wavelengths show what would happen if the point source observation was noisy. The optimally extracted spectrum beyond 26micron behaves much better than the aperture extracted spectrum.

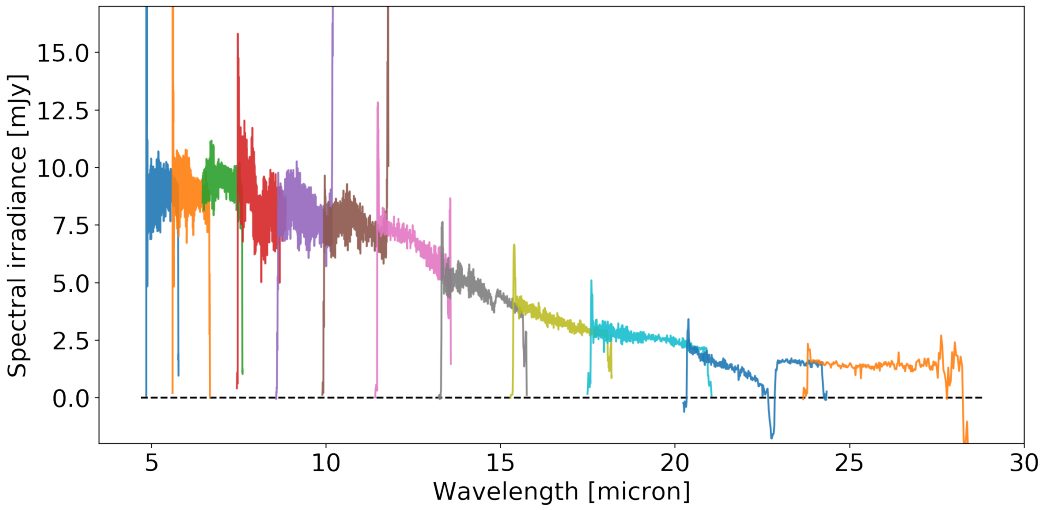

Figure 23. 800K BB point source optimally extracted signal.

5. CONCLUSION AND FUTURE WORK

The peculiarities of MRS detector images were outlined, along with the methods to visualize data spatially and spectrally in detector pixel space. This visualization allows to explain essential definitions such as detector spectral binning and aperture masking. Both of these concepts were used to extract signal from MRS extended source observations. In the case of a point source observation a centroiding algorithm was introduced in order to adequately center the aperture mask onto the point source. The same centroid was used to project the MRS 3D

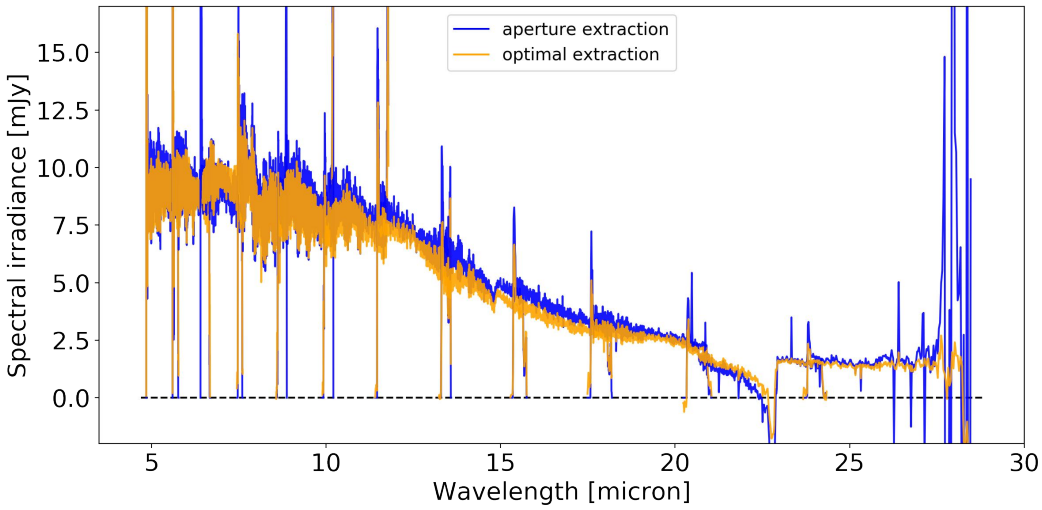

Figure 24. Comparison between the aperture extracted signal and the optimally extracted signal.

PSF onto the 2D detector. The two distinct methods of aperture photometry and optimal spectral extraction were shown to yield promising results. An important extension to the aperture extraction algorithm will be to weigh the pixel contribution based on the fractional area overlap of a pixel with a defined aperture, instead of an all-or-nothing approach. This issue is partially alleviated by applying an aperture correction to the extracted signal.

Although both extraction methods work, they are limited by the current understanding of the MRS calibration. The spectral extraction algorithms can only benefit from an improvement in the calibration steps of the MIRI and MRS pipeline. That is where the bulk of the effort has to be invested.

REFERENCES

[1] Rieke, G. H., Wright, G. S., Böker, T., Bouwman, J., Colina, L., Glasse, A., Gordon, K. D., Greene, T. P., Güdel, M., Henning, T., Justtanont, K., Lagage, P.-O., Meixner, M. E., Nørgaard-Nielsen, H.-U., Ray, T. P., Ressler, M. E., van Dishoeck, E. F., and Waelkens, C., "The Mid-Infrared Instrument for the James Webb Space Telescope, I: Introduction," *PASP* **127**, 584 (July 2015).

[2] Wells, M., Pel, J.-W., Glasse, A., Wright, G. S., Aitink-Kroes, G., Azzollini, R., Beard, S., Brandl, B. R., Gallie, A., Geers, V. C., Glauser, A. M., Hastings, P., Henning, T., Jager, R., Justtanont, K., Kruizinga, B., Lahuis, F., Lee, D., Martinez-Delgado, I., Martínez-Galarza, J. R., Meijers, M., Morrison, J. E., Müller, F., Nakos, T., O'Sullivan, B., Oudenhuysen, A., Parr-Burman, P., Pauwels, E., Rohloff, R.-R., Schmalzl, E., Sykes, J., Thelen, M. P., van Dishoeck, E. F., Vandenbussche, B., Venema, L. B., Visser, H., Waters, L. B. F. M., and Wright, D., "The Mid-Infrared Instrument for the James Webb Space Telescope, VI: The Medium Resolution Spectrometer," *PASP* **127**, 646 (July 2015).

[3] Labiano, A., Azzollini, R., Bailey, J., Beard, S., Dicken, D., García-Marín, M., Geers, V., Glasse, A., Glauser, A., Gordon, K., Justtanont, K., Klaassen, P., Lahuis, F., Law, D., Morrison, J., Müller, M., Rieke, G., Vandenbussche, B., and Wright, G., "The MIRI Medium Resolution Spectrometer calibration pipeline," in [*Observatory Operations: Strategies, Processes, and Systems VI*], *Proceedings of the SPIE* **9910**, 99102W (July 2016).

[4] Horne, K., "An optimal extraction algorithm for CCD spectroscopy," *PASP* **98**, 609–617 (June 1986).